Applied Catalysis B: Environmental 165 (2015) 79–86

Contents lists available at ScienceDirect

Applied Catalysis B: Environmental

journal homepage: www.elsevier.com/locate/apcatb

Highly dispersed Pd/PdO/Fe_2O_3 nanoparticles in SBA-15 for Fenton-like processes: confinement and synergistic effects

Xingfa Li[a,b], Xin Liu[b], Lili Xu[a], Yuezhong Wen[a,c,*], Jianqing Ma[c], Zucheng Wu[b,*]

[a] Institute of Environmental Science, College of Environmental and Resource Sciences, Zhejiang University, Hangzhou 310058, China
[b] Department of Environmental Engineering, State Key Laboratory of Clean Energy Utilization, Zhejiang University, Hang Zhou 310027, China
[c] Zhejiang Provincial Key Laboratory of Organic Pollution Process and Control, Zhejiang University, Hangzhou 310058, China

ARTICLE INFO

Article history:
Received 24 June 2014
Received in revised form 27 August 2014
Accepted 29 September 2014
Available online 6 October 2014

Keywords:
Nanoparticle
Catalyst
Fenton-like reaction
Confinement effect
Synergistic effect.

ABSTRACT

Heterogeneous Pd catalytic Fenton-like systems with in-situ-generated H_2O_2 have recently gained significant attention for wastewater treatment. Intense research efforts have been focused on developing highly efficient Fenton-like catalysts. It is known that nanoparticle size and appropriate coordination of active compositions are important for the fabrication of a highly efficient multicomponent catalyst. Unfortunately, effects of these factors on Fenton-like reaction are still unknown. To decipher the puzzle, we designed multicomponent Pd/PdO/Fe_2O_3 nanoparticles in SBA-15 (denoted as FePd-SBA) as a Fenton-like catalyst which possesses uniform and highly dispersed nanoparticles (small size about 5 nm) in space-confined channels of SBA-15. The fabricated catalyst shows high catalytic activities in Fenton-like reaction for dye degradation. For example, 98.6% removal of dye Acid Red 73 was obtained under in-situ generation of hydrogen peroxide. In contrast, when the catalyst loaded on SiO_2 without channels or pores (FePd–SiO_2) was prepared, and compared with FePd–SBA, FePd–SiO_2 showed noticeably poor performance (51.6%) under same conditions. Obviously, such a difference in results is due to the confinement effect of SBA-15 porous channels. It was also found that Fe and Pd played important roles in the synergistic effect, that is, Pd worked in in-situ H_2O_2 generation and Fe species worked in decompose H_2O_2 to degrade organic pollutants. When we applied this catalyst for Fenton-like reaction with addition of H_2O_2, it was also found that Pd and PdO played important roles and the synergistic effect between Fe and Pd species actually existed in dye removal. The unique nanostructure makes the catalyst to be a novel and welcoming choice for H_2O_2 favorite reactions.

1. Introduction

With the rapid progress in nanotechnology, various nanocatalysts were intensively designed and used for wastewater treatment to achieve various purposes, such as versatility [1], recyclability [2], low cost [3], high activity [4], and so on. In order to obtain good catalytic efficiency, researchers paid more attention on nanoparticles with small size due to the size effect [4–7]. However, nanoparticles tend to aggregate into large particles, leading to deterioration of catalytic performance [5], so preparation of nanocatalyst with homogeneous distribution and size-elected particles is still a challenge [8]. Besides, nanoparticles suffer from the difficulties in separation and/or diffusion in practical applications in wastewater treatment because of too small size [9]. Therefore, it is very desirable to develop a strategy to prepare nanoparticles on suitable matrix in order to get good dispersibility and separability as well as remarkable catalytic activity. Thus, deposition of nanoparticles exclusively on the large surface of oxide materials has been explored such as SiO_2 [10,11], Al_2O_3 [12], TiO_2 [13] and so on, but the exposure of oxide surface resulted in significant loss of treatment efficiency. Because it is difficult to limit the growth of nanoparticles in an open space, uniformity of size and distribution is limited [8].

Recently, ordered mesoporous material SBA-15 has been widely used as the catalyst support in wastewater treatment due to their large structural stability in water [14–17]. It is well known that in order to enhance catalytic activity, active sites should be kept strictly separate and be surrounded exclusively by catalytically inactive substances [18]. In the meantime, hybrid multicomponent nanoparticles can allow separate reaction steps to occur in close proximity at different metal sites and accelerate catalysis [19]. Defined narrow channels of SBA-15 with large surface area, high porosity, ordered and tunable pore size provide a confinement

* Corresponding authors. Tel./fax: +86 571 88982421.
E-mail addresses: wenyuezhong@zju.edu.cn (Y. Wen), wuzucheng@zju.edu.cn (Z. Wu).

http://dx.doi.org/10.1016/j.apcatb.2014.09.071
0926-3373/

environment for nanoparticles. Considerable efforts have been dedicated for embedding active chemical composition into the poles of porous material; however, most of them focused on the adsorption and drug delivery [1,20,21], and few researches have been performed in investigating the confinement effect and nanoparticles distribution with multicomponents for catalytic degradation of organic pollutants in water.

Nowadays, heterogeneous Fenton-like catalysts based on iron have been intensively investigated due to environmental friendliness of H_2O_2 [3,22–24]. However, the major problem of Fenton-like reaction is that only a small percentage of the total H_2O_2 consumption is converted into free •OH [15], and such low efficiency is because H_2O_2 is usually provided by bulk feeding [25]. In addition, it is costly and dangerous for the production, transportation and storage of H_2O_2 [2]. Therefore, in-situ generation of H_2O_2 has attracted much attention and Pd was frequently used [12,13,26,27]. It seems that only the function of Pd in in-situ generation of H_2O_2 was studied, few of the researches reported the synergistic effect between Fe and Pd species in pollutant degradation with in-situ-generated H_2O_2. Besides, little information is available regarding the confinement effect on catalytic degradation of organic pollutants. Therefore, in order to understand the process during the action of the catalyst, the following questions need to be answered:

- Whether uniform and highly dispersed FePd nanoparticles can be obtained by confinement in pores?
- Whether Pd and PdO play their roles in Fenton-like reaction?
- Whether synergistic effect between Fe and Pd species exists in Fenton-like reaction or not and how it works?

Considering all the factors above, we designed a highly active and homogeneously distributed multicomponent Pd/PdO/Fe_2O_3 nanoparticle in SBA-15. Fe_2O_3 was used here to achieve cooperative performance in Fenton-like reaction because it can decompose H_2O_2. Besides, a noble metal-transition metal oxide interface (Pd-on-Fe_2O_3) can be fabricated, which facilitates the activation of reagents and results in improved activities [19,28]. Characterization results showed that the designed catalyst possesses fine nanoparticles, high dispersion and high catalytic activity. Fast degradations of dyes in Fenton-like reaction were obtained through this multicomponent catalyst.

2. Materials and methods

2.1. Materials

Mesoporous silica SBA-15 ($SiO_2/Al_2O_3 \geq 500$; pore diameter: 6–8 nm; BET: 400–600 $m^2\,g^{-1}$) was purchased from Nanjing XFNano Material Tech Co. Ltd., China. SiO_2 (99.5%, 15 ± 5 nm) was supplied by Aladdin industrial Corporation, China. $Fe(NO_3)_3{\cdot}9H_2O$ (AR), $FeCl_3{\cdot}6H_2O$ (AR), $PdCl_2$ (AR), hydrogen peroxide (GR, 30% w/w), formic acid (AR, 98%) and titanium sulfate (CP) were obtained from National Medicines Corporation Ltd. of China. Acid Red 73 (100%, Molecular Formula $C_{22}H_{14}N_4Na_2O_7S_2$, molecular weight 556.48, Colour Index Number 27290, structure is shown in Fig. S1 in Supporting Information) was purchased from Gracia Chemical Technology Co. Ltd., China. Doubly distilled water was used throughout this study.

2.2. Preparation of the catalyst

The catalyst was prepared by incipient wetness impregnation. Before used as support, SBA-15 was dried at 80 °C in a vacuum oven. An acidified $Fe(NO_3)_3$ (or $FeCl_3$) solution as iron precursor was added into SBA-15 progressively and mixed by vigorous agitation. The mixture was aged for 24 h and then dried in an oven at 85 °C overnight. The precipitate was dehydrated at 105 °C for 3 h and calcined at 400 °C in air (or N_2) for 3 h. The calcined solid was impregnated with acidified $PdCl_2$ afterwards, followed by drying and calcining through the same procedure as performed for Fe. Finally, the solid was reduced by H_2 (20 mL/min) at 200 °C (or 300 °C) for 2 h. The reaction conditions listed in brackets were investigated but not best. The optimal catalyst obtained was denoted as FePd–SBA (calcined at 400 °C in air and reduced by H_2 at 200 °C). Correspondingly, the monometallic Fe-SBA and Pd-SBA catalysts were prepared. 5 wt% Fe or 5 wt% Pd was loaded in SBA, respectively. As a reference, the catalyst loaded on SiO_2 without channels or pores was prepared using the same method as FePd–SBA (denoted as FePd–SiO_2).

2.3. Characterization of the catalyst

N_2 adsorption–desorption isotherm was determined by TRISTAR II 3020 instrument (Micromeritics Instrument Corporation, USA), and pore size distribution was determined from desorption branch of the isotherms by the BJH (Barret–Joyner–Hallender) method.

The TEM measurements were performed on a JEM-1230 microscope (JEOL, Japan). In order to better analyze the dispersion and the sizes of the nanoparticles, catalysts were embedded in Spurr's resin and cut into 60 nm thin sections using a microtome. The diameter of nanoparticles was calculated by accounting more than 300 particles.

The XPS spectra were performed on an ESCALAB 250 electron spectrometer (Thermo Electron Corporation, USA) with Al Kα radiation (1486.6 eV). All binding energies were calibrated by using the C 1s peaks at 284.6 eV as references.

The XRD patterns were collected on a XRD-6000 diffractometer (Shimadzu, Japan) with a Cu Kα ray source ($\lambda = 0.154$ nm) at 40 kV and 40 mA. The low-angle XRD patterns were collected at a scanning speed of 0.5°/min over a 2θ range of 0.5–5°, whereas the wide-angle XRD patterns were collected at a scanning speed of 1°/min over a 2θ range of 20–70°.

XANES signals of the Fe K-edge and Pd K-edge were measured using a transmission mode at beamline 14W1 of the Shanghai Synchrotron Radiation Facility (SSRF). The storage ring was operated at 3.5 GeV with a current of 250 mA. Si(111) and Si(311) double-crystal monochromators were used to reduce the harmonic content in the source beam, respectively. Fe and Pd foils were used for energy calibration. The spectra were normalized to get information about the energy position of the edge. The freeware IFEFFIT was used to perform normalization and linear combination fitting in the same way for all spectra.

The surface charges of all the samples were measured by Particle Size and Zeta Potential Analyzer (ZS90, Malvern Instruments Ltd., UK) in aqueous media at different pH values. NaOH and HCl were used for pH adjustment. Before measurement, the solutions were sonicated for 30 min to remove air bubbles.

2.4. Performance tests of the catalyst

In-situ generation of hydrogen peroxide was performed by the method of formic acid and O_2. A 250 mL magnetically stirred three-necked glass reactor with 50 mL Acid Red 73 (AR73) at 100 mg/L and 0.6 g/L of catalyst, a certain amount of formic acid was also used. Oxygen was passed bubbling into the reaction medium with a flow rate of 20 mL/min. Dye concentrations were monitored by sampling at regular time intervals and analyzed using the UV–vis spectrometer. To further verify the in-situ-generated H_2O_2, the solution (deionized water instead of dye) during the reaction was filtrated

and monitored by spectrophotometric determination using titanium sulfate at 400 nm.

Fenton catalytic performance of the catalyst was tested in 100 mL flask, which was sealed and agitated at 150 rpm in a thermostatic shaker maintained at room temperature. The reaction mixture was initiated with 50 mL of AR73 at 200 mg/L and 0.2 g/L of catalyst at the desired pH. In addition to the dye and catalyst, a certain amount of H_2O_2 (30 wt) was added. Dye concentration was monitored by sampling at regular time intervals and analyzed using a Shimadzu UV-2401PC UV–vis spectrometer (Kyoto, Japan) at 509 nm. Before dye completely decolorized, the aqueous solution was withdrawn, the oxidation products and intermediate products were analyzed by GC-MS using a Finnigan Trace DSQ GC-MS instrument equipped with a UA-5 capillary column (30 m × 0.25 mm × 0.25 mm). The preparation processes of the sample and instrument operating conditions for GC-MS analysis were same as the one described in reference [29]. After reaction (1 h), the solution was centrifuged and the supernatant solution was analyzed by ICP-MS instrument (XSENIES, Thermo Fisher Scientific, America). The solid was collected and used in next run. After three reuses, the catalyst was collected, dried at 50 °C in a vacuum oven and characterized by XPS and XRD.

3. Results and discussion

3.1. Location of FePd nanoparticles confined in SBA-15

The porous material can provide confinement environment for orderly growth of nanoparticles, which means that the active chemical composition should be located in the internal poles of the material. Under this condition, BET surface area and pore volume would decrease after catalyst preparation due to the part blockage of the pore system [5,8,17]. For all samples supported by SBA-15 in this study (pure SBA-15, Fe-SBA, Pd-SBA and FePd-SBA), a typical IV isotherm with H1 hysteresis loop at the relative pressure p/p_0 = 0.6–0.7 was observed from the N_2 adsorption–desorption isotherms (not shown), indicating that they still keep a well-defined hexagonal pore structure same as the pure SBA-15. But when metals were introduced in fresh SBA-15, BET surface areas and pore volumes (shown in Table 1) decreased greatly comparing with that of fresh SBA-15, suggesting successful incorporation of metal species inside SBA-15 channels after loading. In contrast, FePd–SiO_2 showed low BET surface area and large pore diameter, which corresponding to its nonporous support.

In order to confirm whether nanoparticles were confined in SBA-15, TEM analyses of pure SBA-15, Fe-SBA, Pd-SBA and FePd-SBA were performed, because the TEM images of the slice can display an entirely direct view of the nanoparticles in the supercage of SBA-15 [8]. From Fig. 1a, it can be seen that the pure SBA-15 has a well-ordered mesoporous channel structure. When Fe, Pd and FePd, respectively, were supported into SBA-15, all the samples loaded on SBA-15 retained the hexagonal porous silica structure (Fig. 1b–d). Obviously, introducing metal species in the channels did not affect the framework of the mesoporous materials. The metal particles were well dispersed throughout the silica framework. Fig. 1b showed that iron oxide in Fe-SBA mainly developed in the forms of dark and rod-like nanowires inside the pores of SBA-15. In contrast, Pd nanoparticles in Pd-SBA are highly dispersed with an average size of about 6 ± 1 nm and uniformly distributed in the channels (Fig. 1c). This result may be attributed to the strong interaction between Pd^{2+} ions and the porous silica, and it was easier to obtain smaller Pd nanoparticles with narrow size distribution compared to Fe nanoparticles. Interestingly, from Fig. 1d, it can be seen that nanoparticles in FePd–SBA have a better uniform and narrow distribution centered at 5.0 nm and the size of particles is significantly smaller than that in Fe–SBA and Pd–SBA. Comparing Fig. 1b with Fig. 1d, it was found that Fe species displayed in the forms of nanowires with tens nm of length when they were incorporated alone in the porous of SBA-15, but nanowires disappeared in the FePd two-component catalyst. That is, there were no obvious separate nanoclusters of Fe species and Pd species in the channels. This phenomenon may be explained by the process that previously formed Fe_2O_3 nanowires partially dissolved and re-precipitated with Pd salt in acidic medium. In the meantime, in order to intuitively reflect the influence of confinement effect on nanoparticle size, the catalyst loaded on SiO_2 without channels or pores was prepared using the same method. From Fig. 1e, obviously, it shows abnormally large size, between 10–60 and 28 nm in average, demonstrating that metal nanoparticle size could be effectively controlled with SBA-15 channels.

XRD characterization can provide some supportive information about the grain size of nanoparticles. Fig. 2A shows the low-angle XRD patterns of pure SBA-15 and FePd–SBA. A typical mesoporous structure with three well-resolved peaks which are indexed as (100), (110) and (200) diffractions were found in two samples, indicating that FePd incorporated SBA-15 is almost the same as the SBA-15 precursor. It should be noticed that the peak (100) for the doped sample shifted slightly to higher 2θ values, indicating that after incorporation the pore size got slightly smaller than the original [17,30]. In the large-angle XRD patterns (Fig. 2B), it can be found obviously that different from of Pd-SBA, shapes of peaks in the FePd–SBA get broad and short, which can be explained by the presence of highly dispersed and small particles, this is highly consistent with the TEM results.

Large-angle XRD patterns (Fig. 2B) are also helpful to identify the crystal phases of FePd–SBA. The broad peaks at about 22° in all samples refer to amorphous silica of SBA-15. For FePd–SBA, diffraction peaks at 33.1°, 35.6°, 49.4°, 54.0°, 62.4° and 63.9°, assigned to (104), (110), (024), (116), (214) and (300) typical characteristic peaks of α-Fe_2O_3 (JCPDS card, File No.89-0597). And the peaks at 40.1° and 46.5°, assigned to (111) and (200) reflections of the cubic Pd lattice (JCPDS card, File No. 46-1043). Beside metallic Pd and α-Fe_2O_3, no other peaks such as Fe–Pd alloy were clearly observed. It can be explained by the close vicinity between metallic Pd and Fe(III) in the channels of FePd–SBA, which causes a strong interaction between Fe species and Pd species and does not lead to the formation of the Fe–Pd alloy [12].

Based on the above analyses, uniform and highly dispersed FePd nanoparticles in SBA-15 were successfully fabricated. Such uniform size and homogeneous distribution mainly originated from confinement environment of SBA-15 pore structures.

Table 1
Structure parameters of all SBA-15 supported samples.

Samples	Surface area (m^2/g)	Pore volume (cm^3/g)	Pore diameter (nm)
Pure SBA-15	558	0.94	5.75
Fe–SBA	414	0.59	5.04
Pd–SBA	411	0.60	5.24
FePd–SBA	369	0.55	4.98
FePd–SiO_2	117	0.68	25.2

3.2. Application for Fenton reaction with in-situ-generated H_2O_2

In-situ generation of H_2O_2 was produced through the reaction of formic acid and O_2. Formic acid is used in this study as a source of hydrogen to produce H_2O_2. According to Yalfani, formic acid can be decomposed over Pd to CO_2 and H_2 (confirmed by the analysis of the overhead gases released during decomposition of HCOOH under Ar atmosphere), which further reacts with O_2 to produce H_2O_2 [31]. The combination of in-situ generation of H_2O_2 and dyes removal

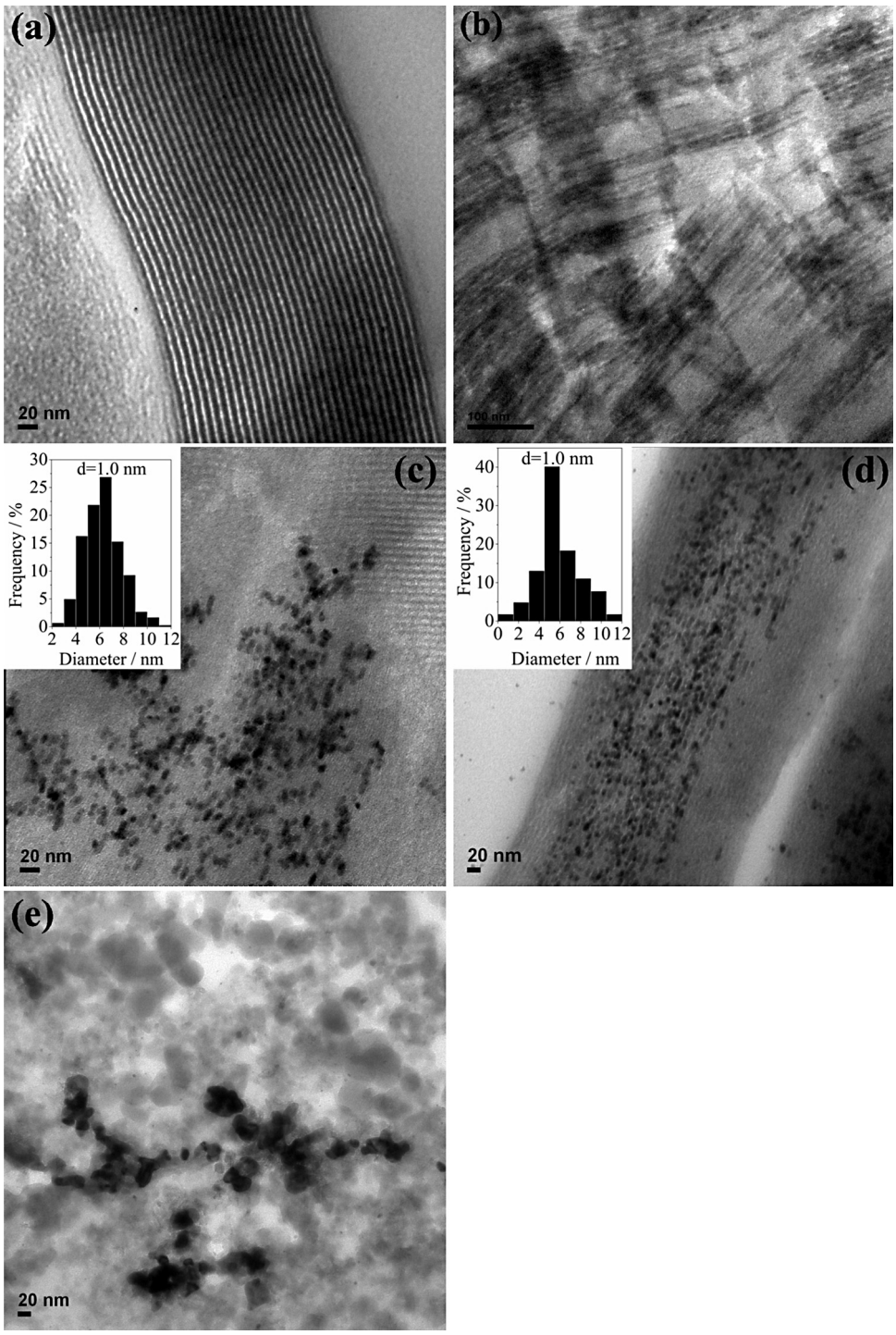

Fig. 1. TEM images of the following samples: (a) pure SBA-15, (b) Fe–SBA, (c) Pd–SBA, (d) FePd–SBA and (e) FePd–SiO_2.

was performed to evaluate catalyst activity. In this study, Acid Red 73 was used as a model reactant, because it is a widely used azo dye in the industries and it is considered to be a bio-refractory pollutant [32–34]. It can be seen from Fig. 3 that catalyst blank (without catalyst, bubbling O_2 in HCOOH added dye solution) exhibited no detectable activity towards dye decolorization. Not surprisingly, when bubbling O_2, no obvious effect in dye removal for the Fe–SBA was observed. Compared to Pd–SBA, the removal rate obtained was 29.5%. But, when FePd–SBA was used, a fast decrease (98.6%) of dye concentration was observed. In order to investigate the adsorption effect of FePd–SBA, the catalyst was used in the absence of formic acid and high removal rate was observed. This means adsorption also accounts for considerable proportion in dye removal. With the increase in time, the gap of dye removal between the presence of formic acid and the absence of formic acid broadened, indicating that degradation reaction happened.

In the meantime, in order to investigate the influence of confinement effect on dye removal, the catalyst FePd–SiO_2 without channels was used. From Fig. 3, comparing with FePd–SBA, FePd–SiO_2 showed noticeably poor performance (51.6%) of catalytic degradation, while displayed strong adsorption (46.2%). Narrow gap of dye removal between the presence of formic acid

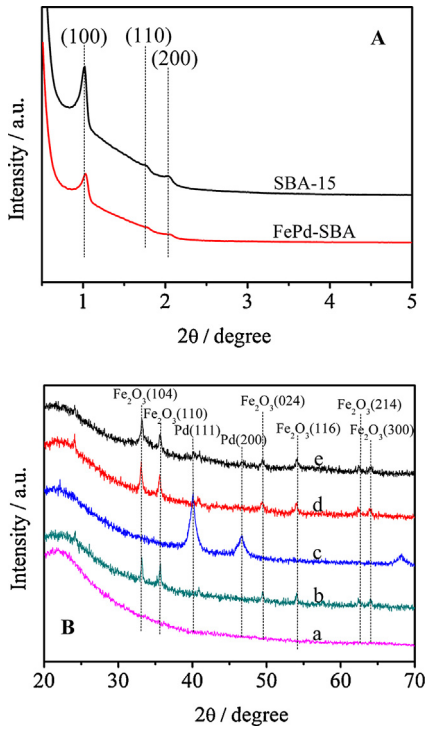

Fig. 2. (A) Low-angle XRD patterns of pure SBA-15 and FePd–SBA. (B) Large-angle XRD patterns of (a) SBA-15, (b) Fe–SBA, (c) Pd–SBA, (d) FePd–SBA and (e) FePd–SBA after reaction.

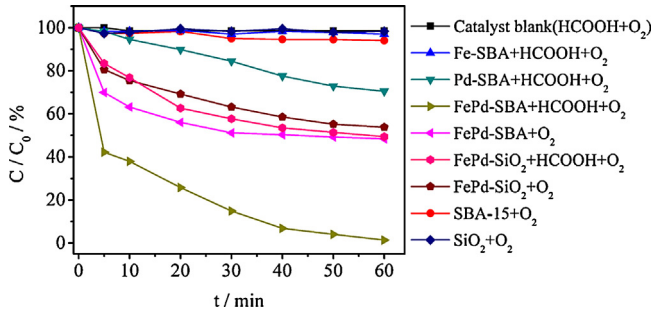

Fig. 3. In-situ generation of hydrogen peroxide for AR73 removal (AR73 100 mg/L, 50 mL, pH 3, catalyst 0.6 g/L, HCOOH 500 mM, O_2 20 mL/min).

and the absence of formic acid indicated weak catalytic activity of FePd–SiO_2. This result can be explained, at least in part, by the broad surface of SiO_2, which lacks a confined structure and thus cannot restrict the growth of nanoparticles, while SBA-15 channels can provide a space-confined nanocage for FePd nanoparticles, resulting in increasing of the local density of active sites [35].

Actually, in the liquid phase of the heterogeneous catalytic reaction, the reactant must first diffuse to the outer surface of the solid catalyst, and then reach the active site and degrade subsequently, so adsorption capacity of a catalyst is vital to its catalytic performance [36]. It is obviously noted that FePd–SBA and FePd–SiO_2 have strong adsorption of the dye. In stark contrast to them, their supports SBA-15 and SiO_2 showed little adsorption although they have large differences in structure and BET surface area. This phenomenon indicated that the strong adsorption of FePd–SBA derived from the active species loaded on it, rather than the support of it. In order to verify this conclusion, zeta-potential and the pH at the point of zero charge (PZC) of the catalyst have been tested, which can be used to address the relation between surface charge of the catalyst and charge of substrate. It can be seen from Fig. S2 that the PZC of FePd–SBA is at pH 3.9, and the surface of FePd–SBA is

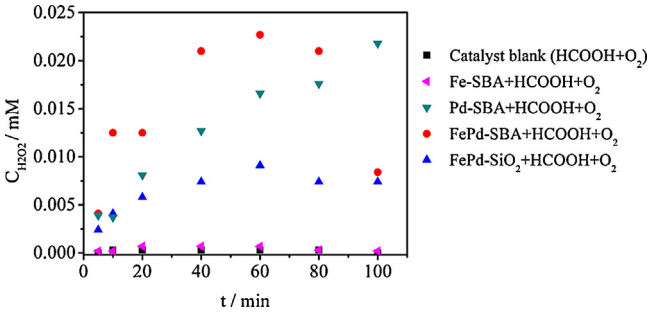

Fig. 4. Directly detect the H_2O_2 by spectrophotometric determination (deionized water 18.0 MΩ cm, 50 mL, pH 3, catalyst 0.6 g/L, HCOOH 500 mM, O_2 20 mL/min).

positively charged at pH 3.0. On the other side, AR 73 is a kind of anionic dye with negative charge at pH 3.0, so it is easily adsorbed on the surface of FePd–SBA via electrostatic interaction. In contrast, the PZC of SiO_2 is less than 3.0 [37,38], which can also be used to explain the poor adsorption of SBA-15 and SiO_2 for the dye.

To further verify the in-situ-generated H_2O_2, the solution (deionized water instead of dye) after reaction was filtrated and the H_2O_2 was determined and shown in Fig. 4. No obvious H_2O_2 was formed in catalyst blank (without catalyst, bubbling O_2 in HCOOH added aqueous solution). Similar phenomenon was also observed when Fe–SBA was used, indicating that Fe does not take part in formic acid decomposition and H_2O_2 formation. This is consistent with the fact that no dye was degraded when Fe–SBA was used as a catalyst. In contrast, high concentrations of H_2O_2 were detected when Pd–SBA, FePd–SBA and FePd–SiO_2 were applied, demonstrating that H_2O_2 only can be generated by Pd contained catalysts in this study. It should be noticed that with increasing time, concentrations of H_2O_2 increased for Pd–SBA, but decreased for FePd–SBA and FePd–SiO_2. This result may be attributed to decomposition of H_2O_2 by Fe species in the latter two catalysts. These results indicated that through the combination of the in-situ generation of H_2O_2 by Pd species and simultaneous decomposition by Fe species, dye can be efficiently removed by cooperation between compositions in FePd–SBA. When FePd–SBA was used, relatively low concentration of H_2O_2 was detected which can also be ascribed to this formation–decomposition process. Weak performance of FePd–SiO_2 in dye removal can be explained by its poor generation ability of H_2O_2 shown in Fig. 4.

It can be seen that the concentrations of H_2O_2 generated by in-situ method seem much smaller than the substrate in the reaction. On the one hand, the concentration of H_2O_2 detected in the study was residual H_2O_2 after decomposed by Pd and Fe species, rather than produced H_2O_2, so the equilibrium concentration of H_2O_2 was not high. On the other hand, the catalytic system involves the simultaneous generation of hydrogen peroxide from formic acid and oxygen, the formation of hydroxyl radicals and the oxidation of dye, the H_2O_2 is provided by consecutive feeding rather than by bulk feeding, so the catalytic system is effective despite low concentration of H_2O_2.

3.3. Application for Fenton-like reaction with addition of H_2O_2

Because as mentioned above, FePd–SBA is an integrated catalyst where there is simultaneous generation of H_2O_2 and efficient degradation of dye. It has been known that Pd plays important role in in-situ H_2O_2 generation, but whether it works in generation of •OH radicals and whether synergistic effects between Fe species and Pd species exist in Fenton-like reaction are not clear. Therefore, we tested the catalyst for dye degradation using Fenton-like reaction without in-situ-generated H_2O_2. H_2O_2 was artificially added into dye solution in the absence of O_2 and formic acid, and the

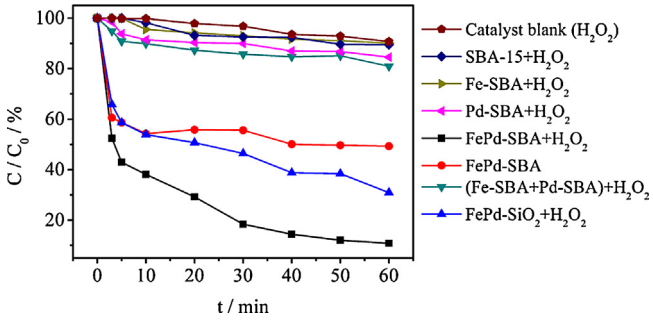

Fig. 5. Fenton degradation of catalysts for AR73 removal (AR73 200 mg/L, 50 mL, pH 3, catalyst 0.2 g/L, H_2O_2 100 mM).

results are shown in Fig. 5. The data of catalyst blank (without catalyst, H_2O_2 added into dye solution) test indicated that there was not much oxidation degradation for dye removal with H_2O_2 alone. Also, there was low dye degradation with SBA-15 and H_2O_2. After metals were supported in SBA-15, weak performances of single-component Fe–SBA (not more than 10% removal in 1 h) and Pd–SBA (about 15% removal) were observed.

However, Fig. 5 indicated that FePd–SBA achieved much more removal rate than that of Fe–SBA and Pd–SBA, respectively. In order to verify the presence of Fenton catalytic degradation, the adsorption effect of FePd–SBA here was also investigated. It can be seen that the gap of dye removal between adsorption (no H_2O_2) and Fenton reaction increases from 8.2% in 3 min to 38.5% in 1 h and continues to increase, indicating that degradation reaction happened. In order to investigate the joint effect of Fe–SBA and Pd–SBA catalysts, equal amounts of Fe–SBA and Pd–SBA were physically mixed (referred as Fe–SBA + Pd–SBA and shown in Fig. 5). According to Fig. 5, it can be seen that the removal of FePd–SBA is far higher than that of their joint, and reaches up to 89.1% for 50 mL of 200 mg/L AR73 in 1 h. These results indicated that the synergistic effect between Fe species and Pd species actually exists in Fenton reaction. In addition, it can also be seen from Fig. 5 that catalytic activity of FePd–SBA is higher than FePd–SiO_2 in removal of refractory pollutant, which once again illustrates the superiority of confinement effect.

In order to further confirm the degradation of dye, the oxidation products and intermediate products were analyzed by GC-MS before dye completely decolorized. The results revealed that the measurable intermediate products were acetic acid, propionic acid, butyric acid, pentanoic acid, phthalic acid, octanoic acid and benzoic acid. These results indicate that the molecules of dye were broken and formed into small-molecule organic acids, and which are known to be biologically degradable.

To test the stability of the catalyst, leached Pd and Fe were measured by ICP-MS after each run, and average of 0.57 and 0.68 mg/L of Pd and Fe were detected after reaction, respectively. Although the concentrations of leached metals was below the limitation of Fe in EU and US (<2 ppm) [39] (no guideline value for Pd in drinking-water was proposed), they were higher than the literature results [25], so the catalyst has relatively high stability.

3.4. Composition identification of active species

In order to further understand the confinement and synergistic effects of catalyst in Fenton reaction, XPS and XANES were used to characterize the chemical composition of active species. From the XPS spectra shown in Fig. 6A, the Fe $2p_{3/2}$ binding energy of 711.8 eV and the corresponding Fe $2p_{1/2}$ peak at 724.9 eV can be solely attributed to the presence of Fe^{3+} ions in α-Fe_2O_3. Meanwhile, signals with binding energies of near 335.1 and 340.5 eV in Fig. 6B belong to Pd $3d_{5/2}$ and Pd $3d_{3/2}$ peaks, that means Pd species

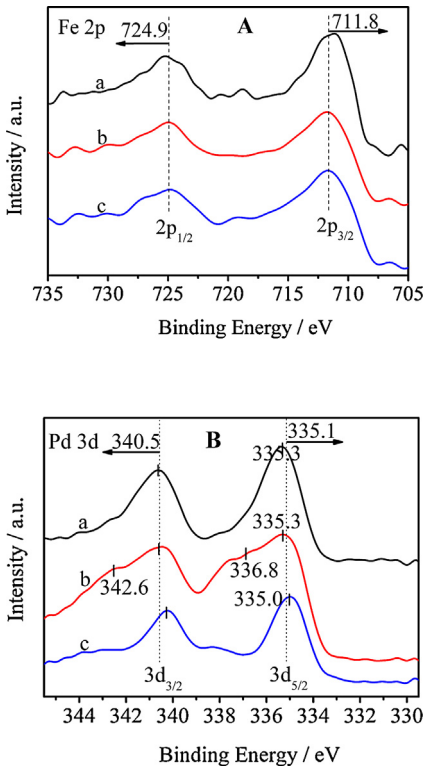

Fig. 6. (A) Fe 2p XPS spectra of (a) Fe–SBA, (b) FePd–SBA and (c) FePd–SBA after reaction; (B) Pd 3d XPS spectra of (a) Pd–SBA, (b) FePd–SBA and (c) FePd–SBA after reaction.

in these samples are mainly metallic Pd. Except for the simple substance of Pd, another broad peaks at 336.8 eV found in FePd–SBA, can be assigned to Pd^{2+} in PdO. These results are in line with the studies of previous researchers [25]. It should also be noted that the Pd $3d_{5/2}$ binding energies of Pd–SBA and FePd–SBA are all slightly higher than the bulk value (335.1 eV) by 0.2 eV. Such shift of binding energy can be explained by the common phenomenon that the binding energy of metal particles decreases with an increase in the particle size, and it finally converges to the bulk value at large particle size [5]. This is highly consistent with the results of confinement effect shown in the TEM images.

In order to investigate the stability of the catalyst, it was characterized after three reuses in Fenton reaction with artificially added H_2O_2. Obviously, the XRD spectra of the catalyst before and after reuses are rather similar (Fig. 2B). Furthermore, it can be seen in Fig. 6 that the peaks of Pd and Fe_2O_3 in the XPS spectra were almost not changed after reaction. These results revealed that the catalyst possesses high stability under reaction conditions, which correspond to the results of leaching measurement by ICP-MS.

Composition of active species can be further verified by the XANES spectra. Determination of the valence state of an atom in a sample can be carried out by comparing the adsorption edge profiles and pre-edge peaks between the sample and reference compounds, because same type of neighbor atoms in nearest coordination shells have similar symmetries and arranges [40]. The local structural environments of iron and palladium in the catalysts, along with the reference materials, are displayed in Fig. 7. It can be seen that the XANES spectra of Fe K-edge in Fe–SBA and FePd–SBA nanoparticles shown in Fig. 7A are similar to that of standard Fe_2O_3 spectrum. Besides, the energy positions and intensities of the pre-edge peaks of the catalysts are also in good agreement with the reference Fe_2O_3, indicating the existence of Fe_2O_3 in the two catalysts. However, it is noteworthy that the main maximum at 7133 eV in FePd–SBA has higher intensity than that in Fe–SBA, which means

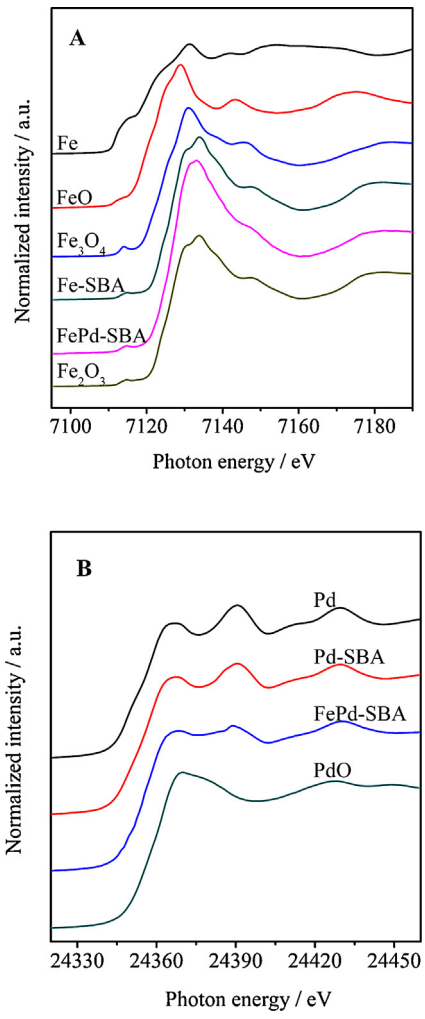

Fig. 7. (A) Fe K-edge XANES spectra and (B) Pd K-edge XANES spectra.

that the former has more empty orbitals than the latter, which might come from the transfer of electron between Fe and Pd which Pd is more electronegative.

Fig. 7B shows that the Pd K-edge in Pd–SBA is energetically similar to that in Pd foil, confirming the presence of zerovalent Pd. While the FePd–SBA exhibits edge shifts between Pd foil and PdO, implying that Pd and PdO coexisted in FePd–SBA. This result is highly consistent with XPS results. To quantify the compositions of Pd–SBA and FePd–SBA, the spectra were fitted with a linear combination of the reference spectra. Quantitative results, along with the contributions of the different references, were displayed in Table 2. From Table 2, we can see that zerovalent Pd is dominant in Pd–SBA, while accounting for smaller part in FePd–SBA. The presence of large amount of PdO in FePd–SBA may be the result of interaction between Pd species and Fe_2O_3. That is, in the presence of iron oxides, the Pd species could not be completely reduced to zerovalent Pd under 200 °C. As expected, no Fe^0 was detected in FePd–SBA, and this can be easily explained by the thermodynamic information. Bond dissociation energies of Fe–O is 409 kJ/mol, while Pd–O is 234 kJ/mol, which means that Fe–O in Fe_2O_3 was harder to crack and to form Fe^0.

Table 2
Linear combination of XANES spectra of SBA-15 supported catalysts.

Reference catalyst	Fe	Pd	
	Fe_2O_3	Pd	PdO
Fe–SBA	100%	/	/
Pd–SBA	/	92.6%	7.4%
FePd–SBA	100%	70.6%	29.4%

According to these above analyses, it can be concluded that the precise fabricated Pd/PdO/Fe_2O_3 nanocatalyst was successfully obtained.

3.5. Possible mechanisms

SBA-15 as a mesoporous material has a defined pore size distribution about 8 nm in this study. Thus, the well-defined Pd/PdO/Fe_2O_3 nanocatalyst can be produced in the confinement environment of channels. The nanoparticle sizes of the multi-component catalyst remain equal to or smaller than the pore sizes of the SBA-15 and are 5 nm in average due to the spatial limitations. Because of the space-confined nanocages and high surface area of the SBA-15, small nanoparticles with homogeneous distribution were obtained. The bimetallic FePd–SBA catalyst gives much higher reaction activity than nonporous FePd–SiO_2 in Fenton reaction, this result is highly consistent with the point that smaller nanoparticles size gives much higher reaction activity [5].

Besides the confinement effect, other factors also contribute to the high activity of the catalyst. First of all, PdO seems play important role in adsorption of the catalyst. From Figs. 3 and 5, it can be observed that there is considerable dye adsorption ability of FePd–SBA. Zeta-potential measurements showed that positively charged catalyst surface is responsible for the strong adsorption. Comparative experiments showed that the strong adsorption has nothing to do with the support SBA-15. In the meantime, from Table 2, it was found that PdO accounts for about 30% of Pd species in FePd–SBA, more than that in Pd–SBA (no more than 8%). Furthermore, FePd–SBA has same amount of Fe_2O_3 as Fe–SBA. Considering the weak dye removals of Fe–SBA and Pd–SBA, it is reasonable to deduce that the adsorption ability comes from PdO. In order to confirm this suppose. Fe-, Pd- and FePd-supported SBA-15 were prepared using the same process as above except that in the end of preparation process, the solid was not reduced by H_2 (referred as Fe–SBA-unreduced, Pd–SBA-unreduced and FePd–SBA-unreduced, respectively) and the adsorption performances of the unreduced samples were shown in Fig.S3. The strong and almost equal adsorptions of dye for Pd–SBA-unreduced and FePd–SBA-unreduced were observed.

Second, Fe and Pd species of the catalyst showed perfect synergistic effects in dye removal. FePd–SBA not only achieved much more removal rate than that of Fe–SBA and Pd–SBA alone, but also far higher than that of their joint. In the dye degradation with in-situ-generated H_2O_2, the catalytic system involves the simultaneous generation of H_2O_2 from HCOOH by Pd species, the decomposition of H_2O_2 into hydroxyl radicals by Fe and Pd species. Close cooperation of the active species makes the reaction system work well despite that low concentration of H_2O_2 was detected in the reaction.

Last but not least, Pd seems to play vital roles in accelerating the decomposition of H_2O_2. On the one hand, Pd is capable of redox cycling and produces •OH in the presence of H_2O_2, because it can catalyze decomposition H_2O_2 without Fe species [31]. On the other hand, the electronegativities of Fe(III) is 1.96 while Pd(0) is 2.20, apparently the Pd(0) will attract electron density from the neighbor iron oxide nanoparticles, behaving likes Lewis acid sites, so the reduction of the Fe(III) to Fe(II) is facilitated and the whole catalytic reaction is accelerated [14].

4. Conclusions

In the present work, a uniform and highly dispersed nanocatalyst was successfully fabricated. Such uniform size and

homogeneous distribution mainly originated from the confinement environment of SBA-15 pore structures. This catalyst displays excellent performances for dye removal by adsorption, in-situ generation of hydrogen peroxide and Fenton catalytic reaction. High activity originates from the combination of confinement effect of porous channels of SBA-15, synergistic effects between Fe species and Pd species and coordination of adsorption and catalysis in Fenton reaction.

Acknowledgements

The authors acknowledge the financial support from 863 Research Project (2013AA065202), the National Natural Science Foundation of China (No. 21377111) and Zhejiang Provincial Natural Science Foundation of China (No. LY12B07006). We also thank the staff at beamlines BL14W at the Shanghai Synchrotron Radiation Facility (SSRF) for providing the beam time and data analysis.

Appendix A. Supplementary data

Supplementary material related to this article can be found, in the online version, at http://dx.doi.org/10.1016/j.apcatb.2014.09.071.

References

[1] Y. Deng, Y. Cai, Z. Sun, J. Liu, C. Liu, J. Wei, W. Li, C. Liu, Y. Wang, D. Zhao, Journal of the American Chemical Society 132 (2010) 8466–8473.
[2] M. Luo, S. Yuan, M. Tong, P. Liao, W. Xie, X. Xu, Water Research 48 (2014) 190–199.
[3] Z. Ai, Z. Gao, L. Zhang, W. He, J.J. Yin, Environmental Science and Technology 47 (2013) 5344–5352.
[4] S. Navalon, R. Martin, M. Alvaro, H. Garcia, Angewandte Chemie-International Edition 49 (2010) 8403–8407.
[5] J. Cai, H. Ma, J. Zhang, Q. Song, Z. Du, Y. Huang, J. Xu, Chemistry - A European Journal 19 (2013) 14215–14223.
[6] G. Yang, N. Tsubaki, J. Shamoto, Y. Yoneyama, Y. Zhang, Journal of the American Chemical Society 132 (2010) 8129–8136.
[7] C. Rossy, J. Majimel, E. Fouquet, C. Delacote, M. Boujtita, C. Labrugere, M. Treguer Delapierre, F.X. Felpin, Chemistry-A European Journal 19 (2013) 14024–14029.
[8] A.H. Lu, J.J. Nitz, M. Comotti, C. Weidenthaler, K. Schlichte, C.W. Lehmann, O. Terasaki, F. Schuth, Journal of the American Chemical Society 132 (2010) 14152–14162.
[9] H.T. Wang, Z.X. Dong, C.Z. Na, ACS Sustainable Chemistry & Engineering 1 (2013) 746–752.
[10] B. Tian, T. Wang, R. Dong, S. Bao, F. Yang, J. Zhang, Applied Catalysis B: Environmental 147 (2014) 22–28.
[11] H. Lee, S. Kim, D.W. Lee, K.Y. Lee, Catalysis Communications 12 (2011) 968–971.
[12] M.S. Yalfani, S. Contreras, F. Medina, J.E. Sueiras, Journal of Hazardous Materials 192 (2011) 340–346.
[13] M. Teranishi, S.i. Naya, H. Tada, Journal of the American Chemical Society 132 (2010) 7850–7851.
[14] C.H. Liu, N.C. Lai, S.C. Liou, M.W. Chu, C.H. Chen, C.M. Yang, Microporous and Mesoporous Materials 179 (2013) 40–47.
[15] S. Navalon, M. Alvaro, H. Garcia, Applied Catalysis B: Environmental 99 (2010) 1–26.
[16] A. Dhakshinamoorthy, S. Navalon, M. Alvaro, H. Garcia, ChemSusChem 5 (2012) 46–64.
[17] Z.J. Wang, Y.B. Xie, C.J. Liu, The Journal of Physical Chemistry C 112 (2008) 19818–19824.
[18] M. Armbrüster, K. Kovnir, M. Friedrich, D. Teschner, G. Wowsnick, M. Hahne, P. Gille, L. Szentmiklósi, M. Feuerbacher, M. Heggen, Nature Materials 11 (2012) 690–693.
[19] G. Chen, Y. Zhao, G. Fu, P.N. Duchesne, L. Gu, Y. Zheng, X. Weng, M. Chen, P. Zhang, C.W. Pao, Science 344 (2014) 495–499.
[20] Y.F. Zhu, S. Kaskel, T. Ikoma, N. Hanagata, Microporous and Mesoporous Materials 123 (2009) 107–112.
[21] P.F. Wang, H.X. Jin, M. Chen, D.F. Jin, B. Hong, H.L. Ge, J. Gong, X.L. Peng, H. Yang, Z.Y. Liu, X.Q. Wang, Journal of Nanomaterials 2012 (2012) 1–7.
[22] J. Shi, Z. Ai, L. Zhang, Water Research 59 (2014) 145–153.
[23] L. Xu, J. Wang, Environmental Science and Technology 46 (2012) 10145–10153.
[24] Z.M. Cui, Z. Chen, C.Y. Cao, L. Jiang, W.G. Song, Chemical Communications 49 (2013) 2332–2334.
[25] M.S. Yalfani, S. Contreras, J. Llorca, M. Dominguez, J.E. Sueiras, F. Medina, Physical Chemistry Chemical Physics: PCCP 12 (2010) 14673–14676.
[26] G. Li, J. Edwards, A.F. Carley, G.J. Hutchings, Catalysis Communications 8 (2007) 247–250.
[27] E.N. Ntainjua, M. Piccinini, S.J. Freakley, J.C. Pritchard, J.K. Edwards, A.F. Carley, G.J. Hutchings, Green Chemistry 14 (2012) 170.
[28] B.R. Cuenya, Thin Solid Films 518 (2010) 3127–3150.
[29] C.S. Shen, Y.Z. Wen, Z.L. Shen, J. Wu, W.P. Liu, Journal of Hazardous Materials 193 (2011) 209–215.
[30] M. Xia, M. Long, Y. Yang, C. Chen, W. Cai, B. Zhou, Applied Catalysis B: Environmental 110 (2011) 118–125.
[31] M.S. Yalfani, S. Contreras, F. Medina, J. Sueiras, Chemical Communications (2008) 3885–3887.
[32] C.S. Shen, Y. Shen, Y.Z. Wen, H.Y. Wang, W.P. Liu, Water Research 45 (2011) 5200–5210.
[33] C.S. Shen, S.F. Song, L.L. Zang, X.D. Kang, Y.Z. Wen, W.P. Liu, L.S. Fu, Journal of Hazardous Materials 177 (2010) 560–566.
[34] Y.Z. Wen, C.S. Shen, Y.Y. Ni, S.P. Tong, F. Yu, Journal of Hazardous Materials 201 (2012) 162–169.
[35] C. Yu, J. He, Chemical Communications 48 (2012) 4933–4940.
[36] R. Gonzalez Olmos, F.D. Kopinke, K. Mackenzie, A. Georgi, Environmental Science and Technology 47 (2013) 2353–2360.
[37] N. Sahai, Environmental Science and Technology 36 (2002) 445–452.
[38] G.A. Parks, Chemical Reviews 65 (1965) 177–198.
[39] X. Yang, X. Xu, J. Xu, Y. Han, Journal of the American Chemical Society 135 (2013) 16058–16061.
[40] N.N. Tušar, D. Maučec, M. Rangus, I. Arčon, M. Mazaj, M. Cotman, A. Pintar, V. Kaučič, Advanced Functional Materials 22 (2012) 820–826.